



ISSN: 2617-6548

URL: www.ijirss.com

Rational design and computational screening of febrifugine analogues as selective MMP inhibitors for osteoarthritis treatment

Sandy Armandha Adianto Djojogugito^{1*}, Paramasari Dirgahayu², Ratih Dewi Yudhani³, Rieva Ermawan⁴

¹Doctoral Program of Medical Sciences, Faculty of Medicine, Universitas Sebelas Maret, Surakarta, Indonesia.

²Department of Parasitology and Mycology, Faculty of Medicine, Universitas Sebelas Maret, Surakarta, Indonesia.

³Department of Pharmacology, Faculty of Medicine, Universitas Sebelas Maret, Surakarta, Indonesia.

⁴Department of Orthopaedic and Traumatology, Dr. Moewardi General Province Hospital, Surakarta, Indonesia.

Corresponding author: Sandy Armandha Adianto Djojogugito (Email: sandyarmandha82@student.uns.ac.id)

Abstract

Osteoarthritis (OA) is a degenerative joint disorder that primarily affects aging populations, resulting in progressive cartilage degradation and joint dysfunction. The pathological role of matrix metalloproteinases (MMPs), particularly MMP-1, MMP-8, and MMP-13, in extracellular matrix breakdown highlights them as attractive therapeutic targets. This study investigated the inhibitory potential of febrifugine analogs against these collagenases using molecular docking and molecular dynamics (MD) simulations. Computational methods were employed to evaluate binding affinities, stability, and pharmacokinetic profiles of the compounds. Among the tested compounds, Compound 19 exhibited the most favorable binding energies, with -118.788 kJ/mol for MMP-8, -96.532 kJ/mol for MMP-13, and -72.528 kJ/mol for MMP-1. Molecular dynamics simulations validated the stability of Compound 19 complexes over a 200 ns trajectory, as indicated by stable root mean square deviation (RMSD) and radius of gyration (Rg) values. The MM/PBSA free energy decomposition analysis revealed significant contributions from van der Waals and electrostatic interactions, further confirming the binding efficiency. Pharmacokinetic assessments showed that Compound 19 adhered to Lipinski's rule of five, with favorable absorption, distribution, metabolism, and excretion (ADME) characteristics. These results highlight Compound 19 as a potent inhibitor with strong selectivity for MMP-8, making it a promising candidate for osteoarthritis therapy. Further experimental validation is required to confirm its efficacy and explore structure-activity relationships for improved selectivity and safety. This study underscores the potential of febrifugine-based analogs in advancing disease-modifying treatments for osteoarthritis.

Keywords: Collagenase inhibitors, Febrifugine analogs, Matrix metalloproteinases (MMPs), Molecular docking and dynamics, Osteoarthritis therapy.

DOI: 10.53894/ijirss.v8i4.8448

Funding: This study received no specific financial support.

History: Received: 30 May 2025 / Revised: 3 July 2025 / Accepted: 7 July 2025 / Published: 10 July 2025

Copyright: © 2025 by the authors. This article is an open access article distributed under the terms and conditions of the Creative Commons Attribution (CC BY) license (<https://creativecommons.org/licenses/by/4.0/>).

Competing Interests: The authors declare that they have no competing interests.

Authors' Contributions: All authors contributed equally to the conception and design of the study. All authors have read and agreed to the published version of the manuscript.

Transparency: The authors confirm that the manuscript is an honest, accurate, and transparent account of the study; that no vital features of the study have been omitted; and that any discrepancies from the study as planned have been explained. This study followed all ethical practices during writing.

Publisher: Innovative Research Publishing

1. Introduction

Osteoarthritis (OA) is a degenerative joint disorder that primarily affects the aging population and individuals with joint injuries. The pathogenesis of OA involves a combination of mechanical and biological factors that disrupt the balance between cartilage degradation and synthesis, leading to joint pain, stiffness, and reduced mobility [1, 2]. The progression of OA is associated with the breakdown of articular cartilage, remodeling of subchondral bone, and chronic synovial inflammation. The loss of cartilage integrity results in increased joint friction, further exacerbating the degradation process and leading to more severe pain and disability [3, 4]. In addition, inflammatory cytokines and oxidative stress contribute to the pathological changes observed in OA, promoting cartilage destruction and synovial inflammation. While current treatments focus on alleviating symptoms, there is no approved therapy that effectively halts or reverses OA progression [5]. This highlights the need for novel therapeutic strategies that target key molecular pathways involved in cartilage degradation. Effective interventions should aim not only to reduce symptoms but also to prevent further deterioration of joint structures [6]. Advancements in drug discovery and computational approaches may offer promising avenues for identifying new OA treatment candidates.

Matrix metalloproteinases (MMPs) are a family of zinc-dependent endopeptidases that degrade extracellular matrix (ECM) components and play a crucial role in osteoarthritis (OA) pathogenesis. Among them, collagenases such as MMP-1, MMP-8, and MMP-13 are responsible for the degradation of type II collagen, which is essential for cartilage integrity [7, 8]. These enzymes are upregulated in OA, leading to the excessive breakdown of cartilage and an imbalance in tissue remodeling. While MMPs are involved in physiological processes such as embryonic development and tissue repair, their overexpression in OA results in irreversible cartilage loss and joint dysfunction [9]. Targeting MMPs has emerged as a promising therapeutic approach for OA treatment, with various inhibitors being explored to mitigate cartilage degradation [10]. However, many broad-spectrum MMP inhibitors have failed in clinical trials due to off-target effects and musculoskeletal toxicity, necessitating the development of more selective inhibitors. Developing small-molecule inhibitors with high specificity for OA-related MMPs remains a crucial goal in the search for disease-modifying OA treatments [11, 12]. Computational screening techniques have been increasingly utilized to design and optimize MMP inhibitors with enhanced selectivity and potency.

Febrifugine analogs have gained attention as potential MMP inhibitors due to their structural similarity to known collagenase inhibitors and their promising bioactivity. Originally derived from *Dichroa febrifuga*, febrifugine is structurally related to halofuginone, a well-known quinazolinone alkaloid that has demonstrated inhibitory activity against collagenase MMP-2 [13, 14]. Halofuginone has been shown to suppress cancer growth, metastasis, and angiogenesis through the inhibition of MMP-2, alongside its regulation of early growth response 1 (Egr-1) and Nab-2, which suppress MMP-2 promoter activity [15]. Given that febrifugine is an analog of halofuginone, it is hypothesized that febrifugine derivatives may also exhibit inhibitory activity against MMPs involved in OA progression [16]. Furthermore, halofuginone's inhibition of Smad3 phosphorylation in the TGF- β signaling pathway and its role in amino acid starvation response suggest additional mechanisms that could be relevant in OA treatment [17]. While previous studies have focused on halofuginone, the potential of febrifugine analogs for MMP inhibition in OA remains unexplored. Identifying specific structural features that contribute to their inhibitory activity could facilitate the rational design of improved febrifugine analogs.

Computational approaches, including molecular docking and molecular dynamics (MD) simulations, provide valuable insights into the binding affinity and stability of small molecules with target proteins [18, 19]. These methods enable the identification of lead compounds with favorable binding interactions within the active sites of MMPs. Molecular docking predicts the binding conformation and affinity of ligands, while MD simulations assess the dynamic stability of protein-ligand complexes under physiological conditions. Previous studies have successfully employed these techniques to evaluate the inhibitory potential of natural compounds, such as curcumin and its metabolites, against collagenases, demonstrating the effectiveness of *in silico* approaches in guiding drug discovery [20]. By integrating these computational methods, researchers can systematically screen potential inhibitors and refine their molecular properties before proceeding to experimental validation. Given the adaptability of febrifugine analogs, their potential for MMP inhibition warrants further computational analysis to identify the most promising candidates [21]. Furthermore, MM/PBSA calculations can provide thermodynamic insights into the stability and energetic favorability of protein-ligand interactions, thereby enhancing the predictive power of computational studies.

In this study, we utilize molecular docking and MD simulations to investigate the inhibitory potential of febrifugine analogs against MMP-1, MMP-8, and MMP-13. The objective is to identify key molecular interactions that contribute to

binding stability and selectivity, which are essential for effective MMP inhibition. Additionally, pharmacokinetic and toxicity assessments are conducted using *in silico* tools to evaluate the drug-likeness and safety profile of the tested compounds. By integrating multiple computational techniques, this research aims to identify promising lead compounds that could serve as a foundation for the development of novel OA therapies, addressing the urgent need for disease-modifying treatments. The findings of this study could provide valuable insights for the rational design of febrifugine-based MMP inhibitors and contribute to the advancement of targeted OA therapies. Future experimental validation will be necessary to confirm the efficacy and safety of the identified lead compounds.

2. Materials and Methods

2.1. Molecular Properties and Drug-Likeness Assessment

To predict the physicochemical properties and drug-likeness of the designed febrifugine derivative compounds, molecular modeling techniques were applied using Lipinski's rule of five, Ghose, Veber, and Egan criteria. The molecular descriptors, including molecular weight, log P (lipophilicity), hydrogen bond donors, and hydrogen bond acceptors, were evaluated using SwissADME web tools [22]. Additionally, computational models assessed the bioavailability score, predicting the likelihood of oral absorption and systemic circulation. The molecular structure optimization was conducted using Spartan'14 (Wavefunction, Inc.), employing the DFT B3LYP (6-31G) method to generate 3D molecular conformations and calculate electronic properties [23]. Key descriptors such as electrostatic potential (ESP), local ionization potential (LIP), and frontier molecular orbitals (FMOs) were visualized to understand charge distribution and molecular reactivity. Moreover, HOMO-LUMO energy gaps were analyzed to determine the chemical stability and reactivity of the compounds [24]. These computational techniques provided insights into the potential pharmacokinetics and bioactivity of the designed molecules, facilitating early-stage drug discovery.

2.2. Pharmacokinetics and ADMET Prediction

The absorption, distribution, metabolism, elimination, and toxicity (ADMET) properties of the compounds were predicted using the pkCSM web server [25]. Gastrointestinal (GI) absorption, blood-brain barrier (BBB) permeability, and liver metabolism (CYP enzyme inhibition) were computed to determine pharmacokinetic potential. Toxicity risks such as hERG inhibition (cardiotoxicity), AMES mutagenicity (genotoxicity), and hepatotoxicity were also evaluated to ensure safety profiling. The interaction with cytochrome P450 enzymes (CYP3A4, CYP2D6, CYP1A2, CYP2C19, and CYP2C9) was assessed to predict drug-drug interaction risks. The analysis provided crucial insights into oral bioavailability, clearance rates, and potential side effects. Furthermore, water solubility, plasma protein binding (PPB), and renal clearance were estimated to refine the selection of lead compounds. These pharmacokinetic evaluations allowed the identification of drug candidates with optimal therapeutic potential while minimizing toxicity concerns.

2.3. Molecular Docking Analysis

Molecular docking simulations were conducted to examine the binding interactions of the ligands with MMP-1 (PDB ID: 2TCL) [26], MMP-8 (PDB ID: 3DPE) [27] and MMP-13 (PDB ID: 5BPA) [28]. The CLC Drug Discovery Workbench (QIAGEN, Aarhus, Denmark) was used to determine the binding affinity and stability of the protein-ligand complexes [29]. The MMFF94 force field was applied to optimize the ligand geometry, and the binding pockets were defined using co-crystallized ligand coordinates from the Protein Data Bank (PDB). The docking scores ranked the compounds based on binding free energy values, and interaction profiles were analyzed to identify hydrogen bonding, hydrophobic contacts, and electrostatic interactions. The docking validation was performed by re-docking co-crystallized ligands and comparing their scores with the designed compounds. Additionally, molecular interaction maps were generated to visualize key residue-ligand interactions. This approach facilitated the identification of promising inhibitors with favorable binding conformations and stability.

2.4. Molecular Dynamics Simulation

To further investigate the stability of protein-ligand complexes, molecular dynamics (MD) simulations were performed using GROMACS 2020.3 software with the AMBER99SB force field [30, 31]. The SPC water model was used to solvate the system, and the particle mesh Ewald (PME) method was applied for long-range electrostatic calculations. The system was first energy-minimized, followed by equilibration under NVT and NPT ensembles for 100 ps each, before executing the 200 ns production MD run at 300 K. The root mean square deviation (RMSD), root mean square fluctuation (RMSF), solvent-accessible surface area (SASA), and radius of gyration (Rg) were monitored to evaluate the conformational stability and flexibility of the protein-ligand complexes. The binding free energy changes were further examined using hydrogen bonding analysis and ligand root mean square displacement (RMSD). The MD trajectories were analyzed using Xmgrace 5.1.25 software, and clustering analysis was conducted to identify dominant binding conformations [32]. These simulations provided valuable insights into ligand dynamics, protein flexibility, and long-term complex stability.

2.5. Free Energy Calculation Using MM/PBSA

The free energy of the binding of complexes was computed using the MM/PBSA method, which integrates molecular mechanics methods with the Poisson-Boltzmann and surface area continuum solvation models [33, 34]. For each protein-ligand complex, the MM/PBSA binding free energy was determined using the following equation: $\Delta G_{\text{bind}} = G_{\text{complex}} - (G_{\text{protein}} + G_{\text{ligand}}) = \Delta E_{\text{MM}} + \Delta G_{\text{PB}} + \Delta G_{\text{nonpolar}} - T\Delta S$, where ΔE_{MM} denotes the gas-phase interaction energy between the ligand and protein, including van der Waals and electrostatic energies. The terms ΔG_{PB} and

$\Delta G_{\text{nonpolar}}$ represent the polar and nonpolar components of solvation-free energies, respectively. The T ΔS component accounts for the conformational entropy change upon ligand binding. A single-trajectory MM/PBSA protocol was applied, utilizing the protein–ligand complex simulation for energy calculations. The MM/PBSA computations were carried out over the final 10 ns of the production MD trajectory, ensuring equilibrium conditions were met. All calculations were performed using the *g_mmpbsa* tool, providing reliable thermodynamic insights into ligand-protein binding interactions. This methodology allowed for the ranking of compounds based on their energetic favorability, aiding in the selection of potential lead inhibitors.

3. Results

3.1. Molecular Properties, Pharmacokinetics, and Genetic Interaction Profiles of Febrifugine Derivatives

Assessing drug-likeness in the early stages of drug discovery is essential for optimizing resources and selecting promising therapeutic candidates. The compounds in this study were evaluated based on Lipinski's rule of five, which considers molecular mass, lipophilicity (log P), hydrogen bond donors, and hydrogen bond acceptors. According to Table 1, Compounds such as Compounds 7, 12, 13, and 14 meet all Lipinski criteria, indicating good oral bioavailability. Conversely, Compounds 20 and 22, although within acceptable molecular mass limits, exhibited high lipophilicity (log P = 3.29), which could affect solubility and permeability. Compounds without violations, particularly Compounds 7 and 12, are strong candidates for further development as orally active drugs. Structural optimization may be necessary for compounds with borderline physicochemical properties to improve their pharmacokinetic performance. Ensuring compliance with Lipinski's rule increases the likelihood of successful drug formulation and systemic bioavailability. These findings highlight the importance of rational drug design in early-stage screening [35].

Table 1.

Evaluation of drug-likeness criteria using lipinski's rule of five for febrifugine derivatives.

Compound Molecule	Molecular Mass	Log P Value (<5)	H-Bond Donors (Max: 5)	H-Bond Acceptors (Max: 10)	Rule of Five Violations (Count)
Compound 7	287.31 g/mol	0.51	2	5	0
Compound 8	288.30 g/mol	-0.13	2	6	1
Compound 9	288.30 g/mol	-0.20	2	6	1
Compound 10	288.30 g/mol	-0.27	2	6	1
Compound 11	288.30 g/mol	-0.08	2	6	1
Compound 12	305.30 g/mol	0.82	2	6	0
Compound 13	305.30 g/mol	0.87	2	6	0
Compound 14	323.29 g/mol	1.04	2	7	0
Compound 15	355.31 g/mol	1.61	2	8	0
Compound 16	355.31 g/mol	1.58	2	8	0
Compound 17	343.42 g/mol	1.75	2	5	0
Compound 18	343.42 g/mol	1.79	2	5	0
Compound 19	378.42 g/mol	1.65	1	6	0
Compound 20	445.43 g/mol	3.29	1	8	0
Compound 21	317.34 g/mol	0.44	2	6	0
Compound 22	445.43 g/mol	3.29	1	8	0

To refine the selection process, additional medicinal chemistry rules, such as Ghose, Veber, and Egan criteria, were applied to assess drug-likeness properties Table 2. Most compounds met these criteria, with Compounds 7, 12, and 13 displaying the most favorable physicochemical characteristics. These results suggest that the selected compounds may possess optimal permeability and bioavailability, enhancing their potential as oral drugs. The bioavailability index remained consistent at 0.55 for all compounds, reinforcing their likelihood of effective systemic circulation. Interestingly, Compounds 8, 9, 10, and 11 failed the Ghose filter due to minor molecular deviations, although these issues may be addressed through structural modifications. Despite these deviations, none of the compounds demonstrated significant violations that would render them unsuitable for further development. The strategic use of multiple drug-likeness criteria helps identify compounds with high therapeutic potential. These assessments are critical in predicting a compound's success in later stages of drug development.

Table 2.

Drug-likeness attributes based on the guidelines of Lipinski, Veber, Ghose, and Egan.

Compound Molecule	Lipinski Criteria	Ghose Criteria	Veber Criteria	Egan Criteria	Bioavailability Index
Compound 7	Yes	Yes	Yes	Yes	0.55
Compound 8	Yes	No	Yes	Yes	0.55
Compound 9	Yes	No	Yes	Yes	0.55
Compound 10	Yes	No	Yes	Yes	0.55
Compound 11	Yes	No	Yes	Yes	0.55
Compound 12	Yes	Yes	Yes	Yes	0.55
Compound 13	Yes	Yes	Yes	Yes	0.55
Compound 14	Yes	Yes	Yes	Yes	0.55
Compound 15	Yes	Yes	Yes	Yes	0.55
Compound 16	Yes	Yes	Yes	Yes	0.55
Compound 17	Yes	Yes	Yes	Yes	0.55
Compound 18	Yes	Yes	Yes	Yes	0.55
Compound 19	Yes	Yes	Yes	Yes	0.55
Compound 20	Yes	Yes	Yes	Yes	0.55
Compound 21	Yes	Yes	Yes	Yes	0.55
Compound 22	Yes	Yes	Yes	Yes	0.55

The pharmacokinetic and toxicity profiles of the tested compounds were evaluated using *in silico* models to predict absorption, metabolism, and potential safety concerns Table 3. Gastrointestinal absorption was high across most compounds, particularly for Compounds 7, 8, and 9, indicating strong potential for oral bioavailability. Blood-brain barrier (BBB) permeability varied significantly, with Compound 19 displaying the highest log BBB value (0.887), suggesting possible central nervous system interactions. Conversely, Compounds 12 and 13 exhibited low BBB permeability, reducing the risk of neurological side effects. Toxicity assessments revealed that none of the compounds exhibited mutagenic effects in the AMES test, which is favorable for safety considerations. However, Compounds 19 and 20 were flagged as potential hERG I channel blockers, raising concerns about their cardiotoxicity. Skin sensitization risks were observed for Compounds 8 and 19, which may limit their application in topical formulations. The absence of hepatotoxicity in most compounds is a positive indicator for their safety profile. These findings underscore the importance of early toxicity screening to mitigate potential risks.

Table 3.*In silico* analysis of pharmacokinetics and toxicity characteristics of febrifugine molecules.

Compound Molecule	Gastrointestinal Absorption	Blood-Brain Barrier Permeability	AMES Mutagenicity Test	hERG Channel Blocker (Class I)	Liver Toxicity	Skin Allergy Potential
Compound 7	0.103	0.637	No	No	No	Yes
Compound 8	0.104	0.781	Yes	No	No	Yes
Compound 9	0.098	0.788	No	No	No	Yes
Compound 10	0.076	0.791	No	No	No	Yes
Compound 11	0.151	0.728	Yes	No	No	Yes
Compound 12	0.015	0.498	Yes	No	No	Yes
Compound 13	0.029	0.535	Yes	No	No	Yes
Compound 14	0.007	0.35	Yes	No	No	Yes
Compound 15	0.011	0.173	Yes	No	No	Yes
Compound 16	0.011	0.166	Yes	No	No	Yes
Compound 17	0.011	0.248	Yes	No	No	Yes
Compound 18	0.01	0.284	No	No	No	Yes
Compound 19	0.104	0.8870	Yes	Yes	No	Yes
Compound 20	0.005	0.796	Yes	Yes	No	Yes
Compound 21	0.235	0.461	No	No	No	No
Compound 22	0.139	0.529	Yes	No	No	No

Metabolic interaction predictions focused on evaluating the role of the compounds as inhibitors or substrates of cytochrome P450 enzymes, crucial for drug metabolism Table 4. Most compounds exhibited minimal inhibitory activity toward CYP enzymes, indicating a lower likelihood of metabolic interference. However, compounds 19 and 22 were identified as potential inhibitors of CYP3A4 and CYP2C9, suggesting possible interactions with co-administered drugs. The absence of CYP2D6 activity across all compounds reduces the risk of complex metabolic complications, supporting

their pharmacokinetic stability. Compounds 7 and 12 demonstrated no significant enzyme-related activity, reinforcing their potential as lead compounds with minimal metabolic concerns. Proper metabolic profiling is crucial in determining a drug's clearance rate and potential side effects. Addressing metabolic concerns in compounds 19 and 22 through structural modifications may improve their therapeutic applicability. These findings highlight the necessity of metabolic screening in drug development.

Table 4.

Febrifugine compounds as inhibitors or substrates for CYP2D6, CYP3A4, CYP1A2, CYP2C19, and CYP2C9 enzymes.

Compound Molecule	CYP3A4 Activity (Substrate)	CYP1A2 Activity (Inhibitor)	CYP2C19 Activity (Inhibitor)	CYP2C9 Activity (Inhibitor)	CYP2D6 Activity (Substrate/Inhibitor)	CYP3A4 Activity (Inhibitor)
Compound 7	No	No	No	No	No	No
Compound 8	No	No	No	No	No	No
Compound 9	No	No	No	No	No	No
Compound 10	No	No	No	No	No	No
Compound 11	No	No	No	No	No	No
Compound 12	No	No	No	No	No	No
Compound 13	No	No	No	No	No	No
Compound 14	No	No	No	No	No	No
Compound 15	No	No	No	No	No	No
Compound 16	No	No	No	No	No	No
Compound 17	No	No	No	No	No	No
Compound 18	No	No	No	No	No	No
Compound 19	No	No	No	No	No/Yes	Yes
Compound 20	No	No	No	No	No	No
Compound 21	No	No	No	No	No	No
Compound 22	No	No	Yes	Yes	No/Yes	Yes

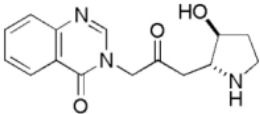
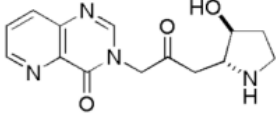
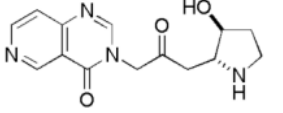
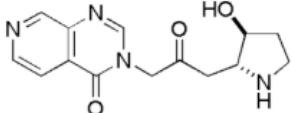
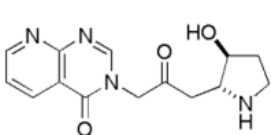
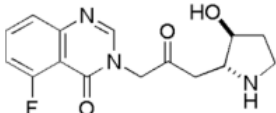
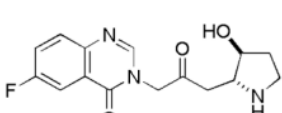
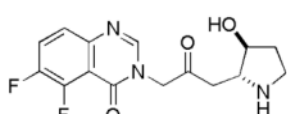
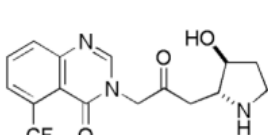
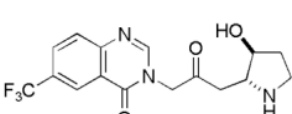
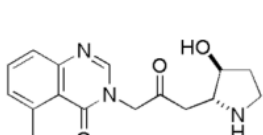
Furthermore, the evaluation of drug-likeness, pharmacokinetics, and toxicity profiles highlights several promising candidates for further research. Compounds 7, 12, and 13 emerged as the most favorable due to their strong compliance with drug-likeness rules, high absorption rates, and minimal toxicity concerns. While Compounds 19 and 22 demonstrated favorable pharmacokinetics, their flagged cardiotoxicity and metabolic interactions necessitate further optimization. Toxicity screening identified potential risks such as skin sensitization and hERG inhibition, emphasizing the need for targeted modifications [36, 37]. The absence of mutagenicity and hepatotoxicity in most compounds supports their potential as safe drug candidates. These findings provide a rational approach for selecting lead compounds while addressing critical pharmacological challenges.

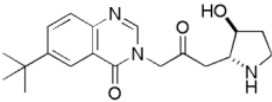
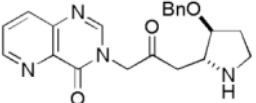
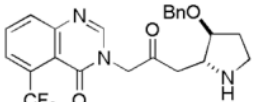
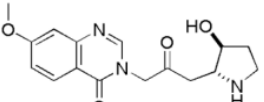
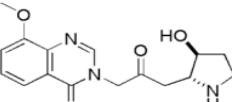
3.2. Computational Docking Analysis and Predicted Ligand-Protein Interaction Profiles

Molecular docking simulations were conducted to examine the interaction patterns and binding affinities of febrifugine derivatives against MMP-1, MMP-8, and MMP-13, key enzymes involved in cartilage degradation. The docking results revealed varying degrees of affinity, with binding free energy values ranging from -7.48 kcal/mol to -11.19 kcal/mol, indicating significant molecular interactions between the ligands and target proteins. Among the tested compounds, Compound 18 exhibited the strongest binding across all three MMP enzymes, highlighting its potential as a potent inhibitor. Additionally, Compounds 13 and 19 demonstrated notable binding to MMP-8 and MMP-13, reinforcing their potential role in osteoarthritis treatment. The docking scores, as detailed in Table 5, suggest that these compounds could serve as promising candidates for further optimization. Understanding the molecular basis of these interactions provides essential insights for developing more selective and potent MMP inhibitors. Given that MMPs are involved in extracellular matrix remodeling, targeting these enzymes effectively could lead to therapeutic advancements in managing osteoarthritis.

Table 5.

Binding affinity analysis of febrifugine derivatives with MMP-1, MMP-8, and MMP-13 enzyme targets.

Compound Molecule	Molecular Structure	Binding Free Energy (MMP-1)	Binding Free Energy (MMP-8)	Binding Free Energy (MMP-13)
Compound 7		-8.56 kcal/mol	-10.74 kcal/mol	-10.61 kcal/mol
Compound 8		-7.81 kcal/mol	-9.91 kcal/mol	-9.89 kcal/mol
Compound 9		-8.02 kcal/mol	-9.46 kcal/mol	-9.84 kcal/mol
Compound 10		-8.09 kcal/mol	-9.77 kcal/mol	-9.89 kcal/mol
Compound 11		-8.48 kcal/mol	-10.32 kcal/mol	-10.02 kcal/mol
Compound 12		-7.83 kcal/mol	-10.35 kcal/mol	-10.54 kcal/mol
Compound 13		-9.31 kcal/mol	-10.65 kcal/mol	-10.24 kcal/mol
Compound 14		-7.70 kcal/mol	-9.98 kcal/mol	-10.50 kcal/mol
Compound 15		-7.48 kcal/mol	-7.81 kcal/mol	-9.92 kcal/mol
Compound 16		-8.20 kcal/mol	-10.37 kcal/mol	-10.72 kcal/mol
Compound 17		-8.53 kcal/mol	-10.84 kcal/mol	-10.07 kcal/mol

Compound 18		-8.60 kcal/mol	-11.19 kcal/mol	-11.15 kcal/mol
Compound 19		-8.79 kcal/mol	-10.59 kcal/mol	-11.02 kcal/mol
Compound 20		-8.35 kcal/mol	-9.96 kcal/mol	-10.74 kcal/mol
Compound 21		-8.31 kcal/mol	-10.15 kcal/mol	-10.69 kcal/mol
Compound 22		-8.27 kcal/mol	-9.85 kcal/mol	-10.69 kcal/mol

The docking analysis identified various molecular interactions that contribute to the stability and specificity of febrifugine derivatives in binding to MMP-1, MMP-8, and MMP-13. The primary stabilizing forces include hydrogen bonding, hydrophobic interactions, and electrostatic contacts, which dictate the overall binding efficiency [38]. For example, Compound 7 formed hydrogen bonds with A: LEU81, A: TYR137, and A: ASN80, while engaging in hydrophobic interactions with A: HIS118 and A: LEU193, reinforcing its stable anchoring within the active site. Similarly, Compound 13 exhibited strong hydrogen bonding with A: ARG114 and A: HIS118, further supporting its potential inhibitory effect. Electrostatic interactions were also present in certain compounds, such as Compound 17, which formed key interactions with A: ARG222, suggesting enhanced specificity toward MMP-8 and MMP-13. The ability of these compounds to engage multiple interaction types enhances their stability, increasing the likelihood of effective inhibition of MMP activity. Notably, Compounds 18 and 19 formed a combination of hydrogen bonds, hydrophobic interactions, and electrostatic contacts, making them strong candidates for further optimization.

A closer analysis of the interaction profiles of high-affinity compounds reveals the critical residues involved in binding stabilization Table 6. Compound 18, which demonstrated the highest binding affinity, established hydrogen bonds with A: HIS228, A: ARG222, and A: GLU219, forming a strong and stable interaction network with MMP-1 and MMP-13. These interactions suggest that the compound effectively occupies the enzyme's catalytic site, which is crucial for enzymatic inhibition. Similarly, Compound 19 formed key hydrogen bonds with A: GLU186, A: TYR215, and A: HIS218, in addition to multiple hydrophobic interactions with A: LEU233 and A: PHE240, which contributed to its strong affinity for MMP-13. Hydrophobic interactions are particularly significant, as they enhance ligand stability within the binding pocket, reducing the likelihood of ligand dissociation. In contrast, Compound 13 displayed a different interaction pattern, forming fewer hydrogen bonds but relying more on π - π stacking interactions with A: HIS228 and A: TYR230, which further stabilized its binding within MMP-8. These structural variations highlight how different compounds exploit unique binding mechanisms to inhibit MMP activity. Understanding these detailed interaction patterns provides essential insights into optimizing Halofuginone derivatives for improved selectivity and potency.

Table 6.

Intramolecular binding interactions of Halofuginone derivatives with MMP-1, MMP-8, and MMP-13 targets.

Compound Molecule	Binding Interaction (MMP-1)		Binding Interaction (MMP-8)		Binding Interaction (MMP-13)	
	Amino Acid Residues	Category	Amino Acid Residues	Category	Amino Acid Residues	Category
Compound 7	A:LEU81 A:TYR137 A:GLY79 A:GLY79 A:ASN80 A:HIS118 A:HIS118 A:VAL115	Hydrogen Bond Hydrogen Bond Hydrogen Bond Hydrogen Bond Hydrogen Bond Hydrophobic Hydrophobic Hydrophobic	A:GLU198 A:ALA161 A:HIS197 A:HIS197 A:ASN218 A:LEU193 A:LEU193 A:LEU214	Hydrogen Bond Hydrogen Bond Hydrophobic Hydrophobic Hydrophobic Hydrophobic Hydrophobic Hydrophobic	A:LEU185 A:ILE243 A:TYR244 A:GLU223 A:ALA186 A:VAL219 A:HIS222 A:HIS222 A:HIS222 A:ILE243 A:LEU239	Hydrogen Bond Hydrogen Bond Hydrogen Bond Hydrogen Bond Hydrogen Bond Hydrogen Bond Hydrogen Bond Hydrophobic Hydrophobic Hydrophobic Hydrophobic
Compound 13	A:LEU81 A:ARG114 A:ARG114 A:ASN80 A:ASN80 A:ALA82 A:GLU119 A:HIS118 A:HIS118 A:VAL115 A:LEU81 A:ALA82 A:VAL115	Hydrogen Bond Hydrogen Bond Hydrogen Bond Hydrogen Bond Hydrogen Bond Hydrogen Bond Electrostatic Hydrophobic Hydrophobic Hydrophobic Hydrophobic Hydrophobic Hydrophobic Hydrophobic	A:LEU160 A:ARG222 A:ALA161 A:GLU198 A:ALA161 A:TYR219 A:HIS197 A:HIS197 A:ASN218 A:ASN218 A:LEU193 A:LEU193	Hydrogen Bond Hydrogen Bond Hydrogen Bond Hydrogen Bond Hydrogen Bond Hydrophobic Hydrophobic Hydrophobic Hydrophobic Hydrophobic Hydrophobic Hydrophobic	A:ALA186 A:GLU223 A:ALA186 A:VAL219 A:HIS232 A:LEU239 A:HIS222 A:HIS222 A:LEU218	Hydrogen Bond Hydrogen Bond Hydrogen Bond Hydrogen Bond Hydrogen Bond Hydrophobic Hydrophobic Hydrophobic Hydrophobic
Compound 17	A:LEU81 A:ALA82 A:TYR140 A:ALA82 A:GLU119 A:ALA82 A:PRO138 A:HIS118 A:TYR110	Hydrogen Bond Hydrogen Bond Hydrogen Bond Hydrogen Bond Hydrogen Bond Hydrogen Bond Hydrogen Bond Hydrogen Bond Hydrophobic	A:ARG222 A:ARG222 A:TYR216 A:LEU214 A:LEU214 A:ALA213 A:LEU214 A:ARG222 A:HIS197 A:LEU193 A:LEU193 A:PRO230 A:LEU193 A:ARG222 A:ARG222	Hydrogen Bond Hydrogen Bond Hydrogen Bond Hydrogen Bond Hydrogen Bond Hydrogen Bond Hydrogen Bond Electrostatic Hydrogen Bond Hydrophobic Hydrophobic Hydrophobic Hydrophobic Hydrophobic	A:THR245 A:THR245 A:THR247 A:THR245 A:ILE243 A:THR245 A:THR245 A:THR245 A:THR247 A:THR247 A:THR247 A:TYR244 A:THR247 A:PHE252 A:LYS249 A:PHE252 A:LYS249 A:LEU218	Hydrogen Bond Hydrogen Bond Hydrogen Bond Hydrogen Bond Hydrogen Bond Hydrogen Bond Hydrogen Bond Hydrogen Bond Hydrogen Bond Hydrogen Bond Hydrogen Bond Hydrophobic Hydrophobic Hydrophobic Hydrophobic Hydrophobic Hydrophobic
Compound 18	A:LEU81 A:TYR140 A:ASN80 A:ASN80 A:GLY79 A:LEU81 A:HIS118 A:VAL115 A:HIS118 A:LEU81	Hydrogen Bond Hydrogen Bond Hydrogen Bond Hydrogen Bond Hydrophobic Hydrophobic Hydrophobic Hydrophobic Hydrophobic	A:LEU160 A:ALA161 A:ASN218 A:TYR219 A:PRO217 A:VAL194 A:GLU198 A:GLU198 A:GLY158 A:TYR219 A:HIS197 A:HIS197 A:TYR219 A:LEU193 A:VAL194	Hydrogen Bond Hydrogen Bond Hydrogen Bond Hydrogen Bond Hydrogen Bond Hydrogen Bond Hydrogen Bond Hydrogen Bond Hydrophobic Hydrophobic Hydrophobic Hydrophobic Hydrophobic Hydrophobic	A:GLU223 A:ALA186 A:GLU223 A:VAL219 A:PHE241 A:LEU239 A:HIS222 A:LEU239 A:PRO255 A:LEU218 A:LEU218 A:LEU239	Hydrogen Bond Hydrogen Bond Hydrogen Bond Hydrogen Bond Hydrophobic Hydrophobic Hydrophobic Hydrophobic Hydrophobic Hydrophobic Hydrophobic

Compound 19	A:LEU81	Hydrogen Bond	A:LEU160	Hydrogen Bond	A:THR245	Hydrogen Bond
	A:ALA82	Hydrogen Bond	A:GLU198	Hydrogen Bond	A:PHE252	Hydrogen Bond
	A:PRO138	Hydrogen Bond	A:GLU198	Electrostatic	A:MET253	Hydrogen Bond
	A:TYR140	Hydrophobic	A:HIS197	Hydrophobic	A:THR247	Hydrogen Bond
	A:HIS118	Hydrophobic	A:ASN218	Hydrophobic	A:HIS222	Hydrophobic
	A:VAL115	Hydrophobic	A:LEU193	Hydrophobic	A:PHE252	Hydrophobic
					A:ILE243	Hydrophobic
					A:LEU218	Hydrophobic
					A:LYS249	Hydrophobic
					A:VAL219	Hydrophobic

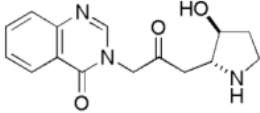
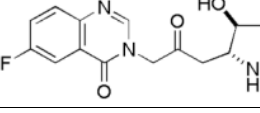
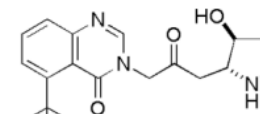
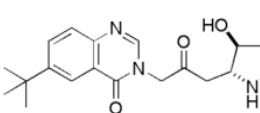
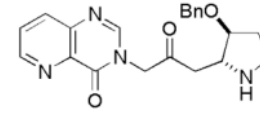
The molecular docking results underscore the potential of febrifugine derivatives as potent inhibitors of MMP-1, MMP-8, and MMP-13, which are key enzymes in osteoarthritis progression. Compounds 18, 13, and 19 emerged as the most promising candidates due to their high binding affinities and well-defined molecular interactions. The combination of hydrogen bonding, hydrophobic, and electrostatic interactions in these compounds suggests a strong inhibitory effect, reinforcing their therapeutic relevance. Future research should focus on optimizing the selectivity of these compounds by modifying functional groups that enhance interactions with key MMP residues while reducing off-target effects. These findings provide a foundation for the development of novel MMP inhibitors targeting extracellular matrix degradation in osteoarthritis. If successfully optimized, febrifugine derivatives could play a significant role in mitigating cartilage degradation and delaying osteoarthritis progression.

3.3. Comprehensive Analysis of Binding Energy and Component Contributions using MM/PBSA

To evaluate the stability and binding potential of ligand-protein complexes, the MM/PBSA method was used to calculate the binding free energy of various compounds. Table 7 summarizes the binding free energy values of Compounds 7, 13, 17, 18, and 19 against three MMP targets: MMP-1, MMP-8, and MMP-13. The results reveal distinct differences in binding energy across the compounds and targets, reflecting their unique interaction profiles. Among these, Compound 19 demonstrated the most favorable binding energy against MMP-8 (-118.788 kJ/mol), followed by MMP-13 (-96.532 kJ/mol) and MMP-1 (-72.528 kJ/mol). Comparatively, Compound 18 showed weaker binding energy, particularly with MMP-1 (-39.977 kJ/mol). These variations in binding energy highlight the differential affinities of each compound towards the three MMP targets. The binding free energy indicates the overall thermodynamic stability of the ligand-receptor complex, with more negative values suggesting stronger binding interactions. This analysis underscores the potential of Compound 19, especially for MMP-8, as a promising candidate for further investigation and optimization.

Table 7.

Energetic evaluation of ligand-receptor binding using MM/PBSA (kJ/mol).

Compound Molecule	Molecular Structure	Binding Free Energy (MMP-1)	Binding Free Energy (MMP-8)	Binding Free Energy (MMP-13)
Compound 7		-33.347 kJ/mol	-84.713 kJ/mol	-28.692 kJ/mol
Compound 13		-53.905 kJ/mol	-73.356 kJ/mol	-76.631 kJ/mol
Compound 17		-71.391 kJ/mol	-91.931 kJ/mol	-92.620 kJ/mol
Compound 18		-39.977 kJ/mol	-105.642 kJ/mol	-80.245 kJ/mol
Compound 19		-72.528 kJ/mol	-118.788 kJ/mol	-96.532 kJ/mol

The binding energy of the ligand-receptor complexes was decomposed into four key components: van der Waals energy, electrostatic energy, polar solvation energy, and non-polar solvation energy Table 8. For Compound 19, van der Waals energy was the largest contributor to binding stability, with the strongest interaction observed for MMP-8 (-231.835 kJ/mol). This suggests that hydrophobic interactions play a significant role in the binding of Compound 19 to MMP-8. Electrostatic energy also contributed favorably, with MMP-13 showing the highest electrostatic interaction (-60.164 kJ/mol), indicating the importance of charge complementarity in this target. However, polar solvation energy acted as a hindrance across all interactions, particularly for MMP-13 (193.324 kJ/mol), reducing the overall binding strength. Non-polar solvation energy remained slightly favorable and relatively consistent, ranging from -11.736 kJ/mol to -18.681 kJ/mol for different targets. These findings reveal that the binding stability of Compound 19 with different MMPs is predominantly driven by van der Waals and electrostatic interactions, while polar solvation energy opposes binding. Such detailed insights into energy contributions are critical for understanding and optimizing ligand design for specific targets.

Table 8.

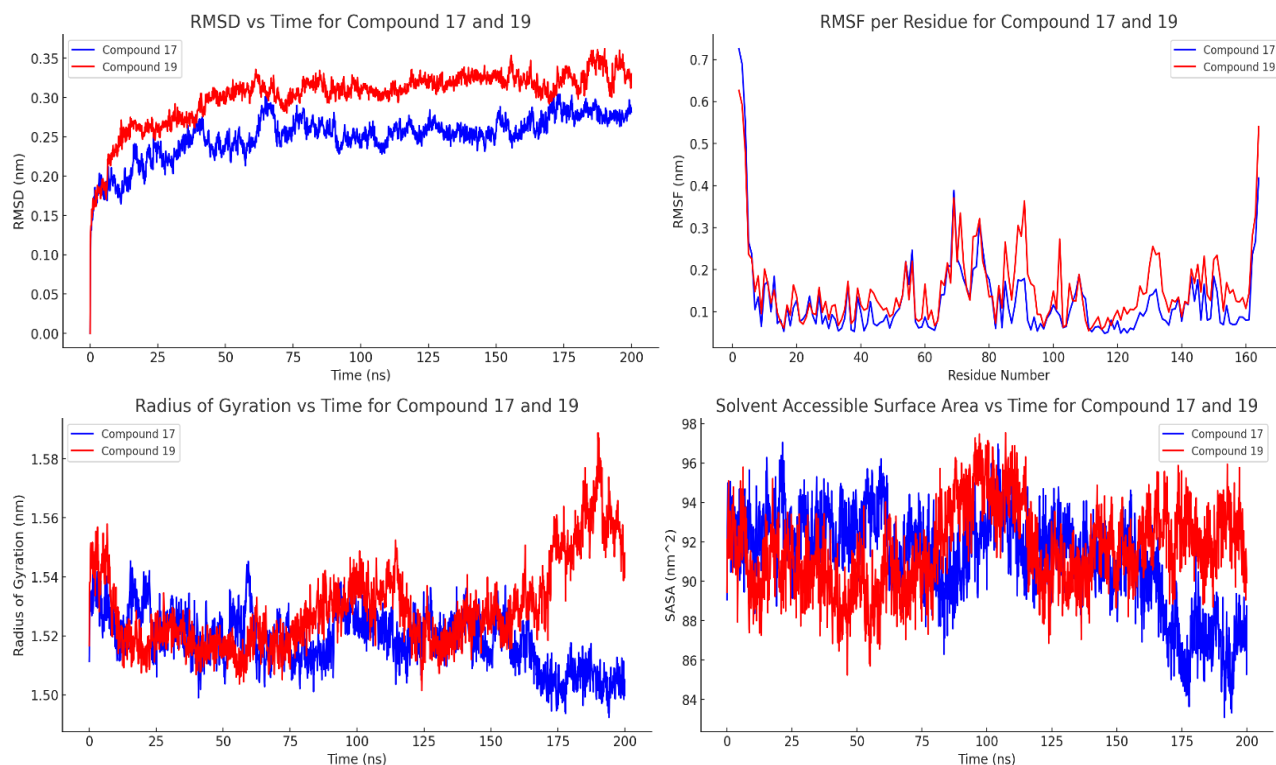
Binding energy components of Compound 19 with different MMP targets (kJ/mol).

Parameters	Compound 19 - MMP-1	Compound 19 - MMP-8	Compound 19 - MMP-13
Delta Van Der Waals Energy	-139.719 kJ/mol	-231.835 kJ/mol	-211.311 kJ/mol
Delta Electrostatic Energy	-25.703 kJ/mol	-24.235 kJ/mol	-60.164 kJ/mol
Delta Polar Solvation Energy	104.629 kJ/mol	155.963 kJ/mol	193.324 kJ/mol
Delta Non-Polar Solvation Energy	-11.736 kJ/mol	-18.681 kJ/mol	-18.382 kJ/mol
Total Binding Energy	-72.528 kJ/mol	-118.788 kJ/mol	-96.532 kJ/mol

The results demonstrate that Compound 19 exhibits selective binding potential, particularly for MMP-8, as evidenced by its highly negative binding energy. The stronger van der Waals and non-polar solvation contributions for MMP-8 suggest that this target provides a more favorable hydrophobic environment for Compound 19. Although MMP-13 showed notable electrostatic contributions, its higher polar solvation energy offset the favorable interactions, leading to weaker overall binding compared to MMP-8. In contrast, MMP-1 exhibited the weakest binding energy with Compound 19, likely due to less favorable interactions in both van der Waals and electrostatic components. These findings emphasize the importance of optimizing hydrophobic and electrostatic interactions to enhance binding affinity and selectivity. Compound 19's selective binding for MMP-8 positions it as a potential candidate for developing specific inhibitors targeting this enzyme. The insights gained from this study can also guide the design of analogs with improved binding properties. Furthermore, this analysis highlights the potential of computational methods, such as MM/PBSA, in rational drug design and target-specific ligand optimization.

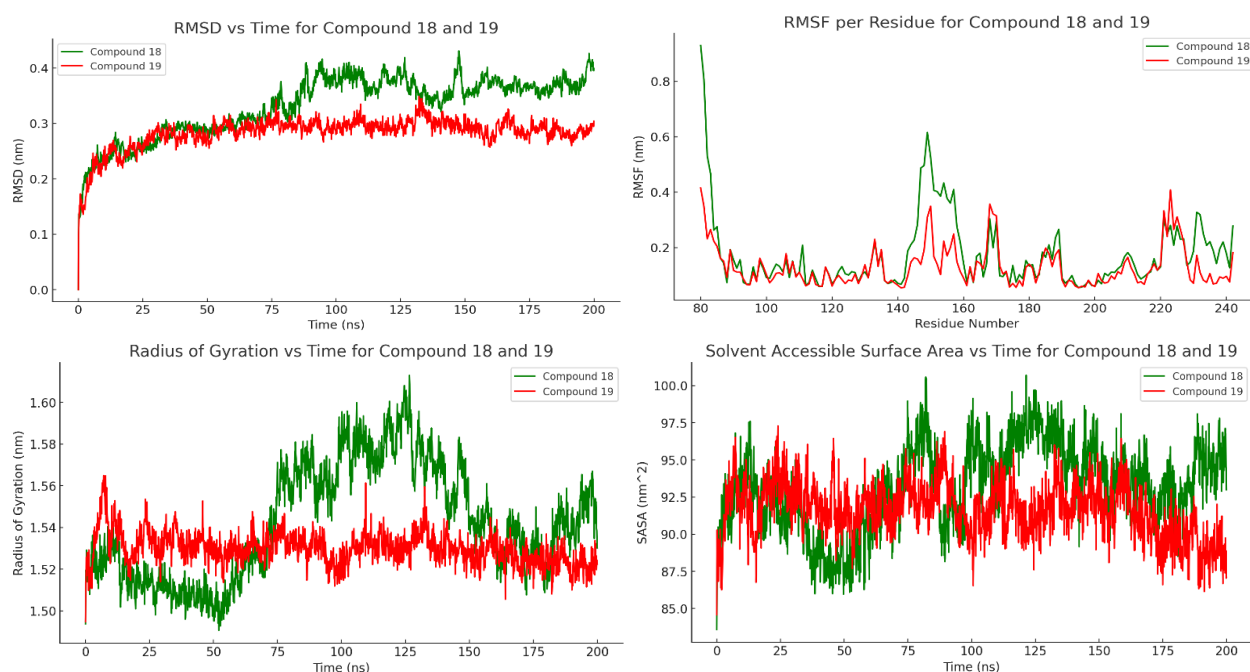
3.4. Stability Analysis of Ligand-Protein Dynamic Interactions

The molecular dynamics simulations for compounds 17 and 19 interacting with MMP-1 are presented in Figure 1. The RMSD values for both compounds stabilized after an initial fluctuation, ranging between 0.25–0.35 nm throughout the simulation. Compound 19 exhibited slightly higher RMSD values compared to compound 17, suggesting minor conformational adjustments during binding. RMSF analysis showed reduced flexibility in the binding site residues for both compounds, confirming stabilization of the active region upon ligand binding. The Rg values for these complexes remained consistent, ranging between 1.54–1.56 nm, indicating compactness and structural stability. SASA analysis demonstrated steady values between 88 and 98 nm², highlighting the maintenance of hydrophobic interactions. Compound 17 showed slightly better stability and structural integrity compared to compound 19, as evidenced by its more consistent RMSD and SASA values. Both compounds effectively stabilized the protein, but compound 17 exhibited superior compactness during the simulation. These results validate the potential of both compounds as MMP-1 inhibitors, with compound 17 performing slightly better. Moreover, the findings highlight the robust interactions formed by these compounds, underscoring their therapeutic promise.

**Figure 1.**

Dynamic molecular simulations were conducted for the two complexes interacting with MMP-1.

Figure 2 illustrates the molecular dynamics simulation results for compounds 18 and 19 interacting with MMP-8. RMSD values for these complexes ranged from 0.20–0.40 nm, with compound 18 exhibiting slightly greater fluctuations than compound 19. This indicates that compound 18 underwent more conformational adjustments during binding but remained stable overall. RMSF analysis revealed that binding site residues in MMP-8 were stabilized for both compounds, with lower flexibility observed compared to other regions. The Rg values for compounds 18 and 19 fluctuated between 1.53–1.58 nm, suggesting compact and stable structures throughout the simulation. SASA values for the two complexes ranged from 90 to 98 nm², indicating consistent hydrophobic interactions with minimal solvent exposure. Compound 19 demonstrated better overall stability compared to compound 18, as reflected in its steadier Rg and SASA values. These findings emphasize that compound 19 exhibited stronger binding affinity and stability for MMP-8. Compound 18, while stable, showed slightly weaker hydrophobic interactions and compactness compared to compound 19. These results suggest that compound 19 is a more promising candidate for targeting MMP-8 due to its superior dynamic behavior.

**Figure 2.**

Dynamic molecular simulations were conducted for the two complexes interacting with MMP-8.

The molecular dynamics simulations for compounds 17 and 19 interacting with MMP-13 are shown in Figure 3. RMSD values for these complexes fluctuated between 0.30–0.50 nm, with compound 19 showing slightly greater stability than compound 17. RMSF analysis highlighted reduced flexibility in the binding site residues for both compounds, indicating stabilization of the active region. The Rg values for both compounds fluctuated between 1.52–1.64 nm, reflecting compact and stable protein-ligand complexes throughout the simulation. SASA analysis revealed values ranging from 85–110 nm², with compound 17 showing slightly greater variations due to transient exposure of hydrophobic residues. Compound 19 exhibited more consistent SASA values, reflecting stronger hydrophobic interactions and better structural integrity during the simulation. Both compounds demonstrated effective binding with MMP-13, but compound 19 displayed superior binding stability. The stabilization of binding site residues and maintenance of compact structures indicate strong protein-ligand interactions for both compounds. Compound 17 formed robust interactions but was slightly less stable compared to compound 19. These findings validate the potential of compounds 17 and 19 as effective MMP-13 inhibitors, with compound 19 emerging as a stronger candidate.

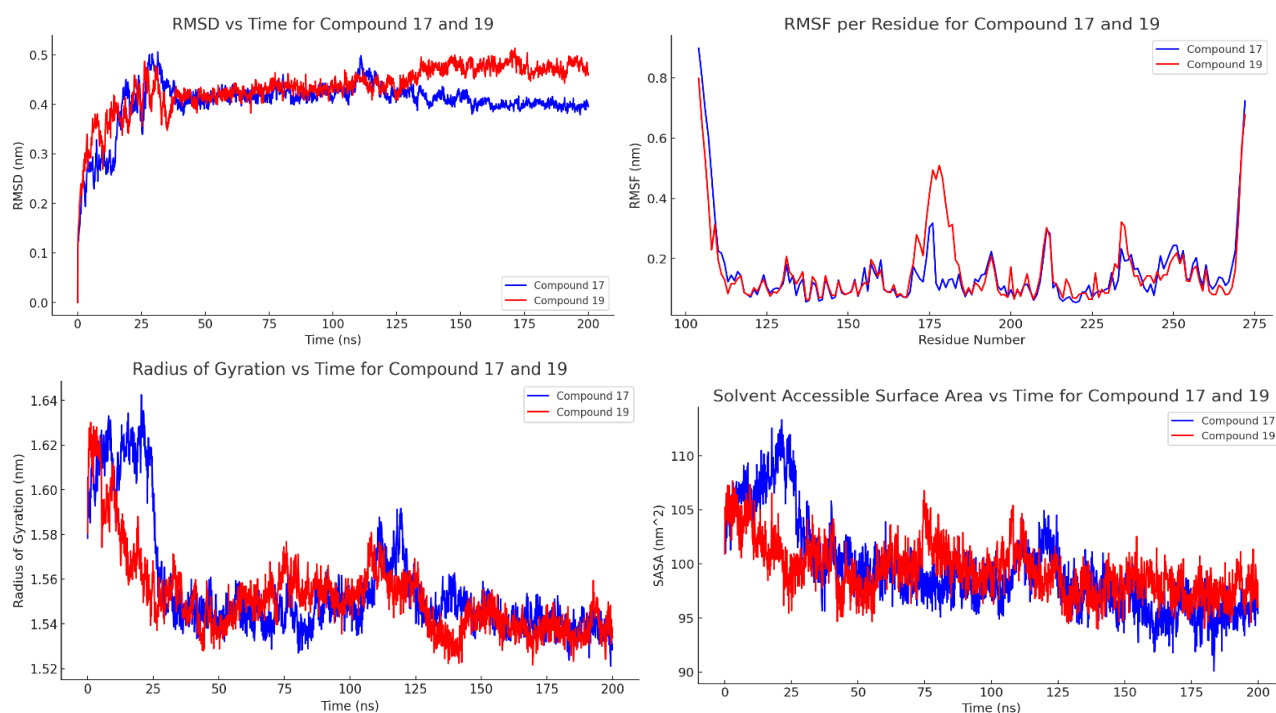


Figure 3. Dynamic molecular simulations were conducted for the two complexes interacting with MMP-13.

The molecular dynamics simulations for MMP-1, MMP-8, and MMP-13 provide critical insights into the stability and dynamics of protein-ligand complexes. RMSD analysis confirmed stable binding across all systems, with compound 19 consistently showing the lowest fluctuations. RMSF analysis revealed stabilization of binding site residues across all complexes, with minimal flexibility observed in the active regions. Rg values remained consistent, indicating that the protein-ligand complexes maintained compactness and structural stability throughout the simulations. SASA analysis demonstrated steady hydrophobic interactions, with compound 19 exhibiting the most consistent values across all metalloproteinases. Among the three compounds, compound 19 emerged as the most stable and selective ligand, particularly in its interactions with MMP-8. Compound 17 showed excellent stability in MMP-1 and MMP-13, while compound 18 demonstrated moderate stability in MMP-8. These findings emphasize the importance of optimizing hydrophobic and electrostatic interactions to enhance binding affinity. This study highlights the utility of molecular dynamics simulations in rational drug design and target-specific ligand optimization.

4. Discussions

Molecular docking and molecular dynamics simulations were conducted to assess the binding stability and interaction mechanisms of selected compounds with MMP-1, MMP-8, and MMP-13. The docking analysis revealed that the compounds exhibited varying degrees of affinity toward the metalloproteinases, with binding free energy values ranging from −7.48 kcal/mol to −11.19 kcal/mol. Among the tested compounds, Compound 18 displayed the strongest binding affinity across all three MMP enzymes, suggesting its potential as a potent inhibitor. The MM/PBSA analysis further supported these findings by quantifying the energetic contributions of van der Waals forces, electrostatic interactions, and solvation effects in ligand binding. The results indicated that Compound 19 exhibited the most favorable binding energy with MMP-8 (−118.788 kJ/mol), followed by MMP-13 (−96.532 kJ/mol) and MMP-1 (−72.528 kJ/mol). These differences highlight the selective binding potential of Compound 19, particularly for MMP-8, which could make it a strong candidate for further optimization in targeted drug design.

The molecular dynamics (MD) simulations provided additional insights into the stability of the protein-ligand complexes under physiological conditions. Root mean square deviation (RMSD) analysis demonstrated that the complexes remained stable throughout the simulation, with fluctuations within an acceptable range. Compound 19 consistently showed the lowest RMSD fluctuations, suggesting a strong and stable interaction with the MMP active sites. The radius of gyration (Rg) values indicated that all protein-ligand complexes maintained their compactness, confirming that ligand binding did not induce significant structural deviations. The solvent-accessible surface area (SASA) analysis revealed stable hydrophobic interactions, with Compound 19 maintaining the most consistent SASA values across all metalloproteinases. The root mean square fluctuation (RMSF) analysis further confirmed that binding site residues exhibited minimal flexibility, indicating that ligand binding effectively stabilized the active regions of the MMP enzymes. These findings validate the use of molecular docking and MD simulations in predicting protein-ligand interactions and highlight Compound 19 as a promising selective inhibitor of MMP-8.

The drug-likeness evaluation using Lipinski's Rule of Five, Ghose, Veber, and Egan criteria indicated that Compounds 7, 12, and 13 exhibited the most favorable physicochemical properties for oral bioavailability. Meanwhile, Compounds 19 and 22, despite showing high binding affinity, displayed potential pharmacokinetic limitations, including high lipophilicity and cardiotoxicity risks (hERG channel blocking effects). In silico ADMET predictions further suggested that most tested compounds demonstrated high gastrointestinal absorption and minimal liver toxicity, reinforcing their potential as orally bioavailable drugs. However, Compound 19 was flagged as a possible hERG I channel blocker, suggesting that structural modifications may be required to mitigate potential cardiotoxic effects. Additionally, Compound 22 demonstrated inhibitory activity against CYP3A4 and CYP2C9, suggesting possible metabolic interactions that may impact co-administered drugs. These findings highlight the importance of optimizing the pharmacokinetic and toxicity profiles of these compounds before advancing them to in vivo validation.

Finally, the results indicate that Compound 19 is the most promising inhibitor for MMP-8, based on its strong binding affinity, stability in MD simulations, and selective interactions with key residues. While Compound 18 also exhibited high binding potential, its binding stability in MMP-1 was significantly lower compared to MMP-8 and MMP-13. These findings emphasize the importance of optimizing hydrophobic and electrostatic interactions to enhance binding affinity and selectivity. Further computational and experimental validation is necessary to confirm the inhibitory activity of these compounds and explore structure-activity relationships (SARs). This study highlights the utility of molecular docking, MM/PBSA, and MD simulations in rational drug design and provides valuable insights for developing novel MMP inhibitors targeting osteoarthritis progression.

5. Conclusions

The molecular docking and molecular dynamics simulations confirmed that Compound 19 exhibited the strongest binding affinity and stability, particularly with MMP-8, making it the most promising candidate for metalloproteinase inhibition. Additionally, Compounds 17 and 18 showed stable interactions, with Compound 17 demonstrating higher affinity toward MMP-1 and MMP-13. ADMET predictions indicated that Compounds 7, 12, and 13 had the most favorable pharmacokinetic properties, while Compounds 19 and 22 showed potential cardiotoxic risks that require further optimization. The findings support Compound 19 as a selective MMP-8 inhibitor, which could be further explored for osteoarthritis treatment. Future studies should focus on experimental validation, structure-activity relationship (SAR) analysis, and lead optimization to enhance binding affinity, pharmacokinetics, and safety. These results highlight the value of computational approaches in predicting protein-ligand interactions, which can aid in the rational design of effective metalloproteinase inhibitors.

References

- [1] V. Di Nicola, "Degenerative osteoarthritis a reversible chronic disease," (in eng), *Regenerative Therapy*, vol. 15, pp. 149-160, Dec 2020. <https://doi.org/10.1016/j.reth.2020.07.007>
- [2] Y. He *et al.*, "Pathogenesis of osteoarthritis: Risk factors, regulatory pathways in chondrocytes, and experimental models," (in eng), *Biology* vol. 9, no. 8, Jul 29 2020. <https://doi.org/10.3390/biology9080194>
- [3] S. Saha and N. Y. Rebouh, "Anti osteoarthritis mechanism of the nrf2 signaling pathway," *Biomedicines*, vol. 11, no. 12, p. 3176, 2023. <https://doi.org/10.3390/biomedicines11123176>
- [4] Q. Yao *et al.*, "Osteoarthritis: Pathogenic signaling pathways and therapeutic targets," *Signal Transduction and Targeted Therapy*, vol. 8, no. 1, p. 56, 2023.
- [5] Z. Ouyang *et al.*, "Cartilage-related collagens in osteoarthritis and rheumatoid arthritis: From pathogenesis to therapeutics," *International Journal of Molecular Sciences*, vol. 24, no. 12, p. 9841, 2023.
- [6] J. Lin *et al.*, "Recent advances in small molecule inhibitors for the treatment of osteoarthritis," *Journal of Clinical Medicine*, vol. 12, no. 5, p. 1986, 2023.
- [7] G. A. Cabral-Pacheco *et al.*, "The roles of matrix metalloproteinases and their inhibitors in human diseases," *International Journal of Molecular Sciences*, vol. 21, no. 24, p. 9739, 2020.
- [8] E.-S. E. Mehana, A. F. Khafaga, and S. S. El-Blehi, "The role of matrix metalloproteinases in osteoarthritis pathogenesis: An updated review," *Life Sciences*, vol. 234, p. 116786, 2019. <https://doi.org/10.1016/j.lfs.2019.116786>
- [9] A. Mukherjee and B. Das, "The role of inflammatory mediators and matrix metalloproteinases (MMPs) in the progression of osteoarthritis," *Biomaterials and Biosystems*, vol. 13, p. 100090, 2024. <https://doi.org/10.1016/j.bbiosy.2024.100090>
- [10] Q. Hu and M. Ecker, "Overview of MMP-13 as a promising target for the treatment of osteoarthritis," *International Journal of Molecular Sciences*, vol. 22, no. 4, doi: <https://doi.org/10.3390/ijms22041742>.
- [11] J. Park and S. Y. Lee, "A review of osteoarthritis signaling intervention using small-molecule inhibitors," *Medicine*, vol. 101, no. 32, 2022. <https://doi.org/10.1097/MD.00000000000029501>

- [12] D. Liu *et al.*, "Small molecule inhibitors of osteoarthritis: Current development and future perspective," *Frontiers in Physiology*, vol. 14, p. 1156913, 2023. <https://doi.org/10.3389/fphys.2023.1156913>
- [13] S. Zhu, Q. Zhang, C. Gudise, L. Wei, E. Smith, and Y. Zeng, "Synthesis and biological evaluation of febrifugine analogues as potential antimalarial agents," *Bioorganic & Medicinal Chemistry*, vol. 17, no. 13, pp. 4496–4502, 2009. <https://doi.org/10.1016/j.bmc.2009.05.011>
- [14] S. Jiang *et al.*, "Antimalarial activities and therapeutic properties of febrifugine analogs," *Antimicrobial Agents and Chemotherapy*, vol. 49, no. 3, pp. 1169–1176, 2005. <https://doi.org/10.1128/aac.49.3.1169-1176.2005>
- [15] E. Zcharia *et al.*, "Inhibition of matrix metalloproteinase-2 by halofuginone is mediated by the Egr1 transcription factor," *Anti-Cancer Drugs*, vol. 23, no. 10, 2012. <https://doi.org/10.1097/CAD.0b013e328357d186>
- [16] M. Pines and I. Spector, "Halofuginone —the multifaceted molecule," *Molecules*, vol. 20, no. 1, pp. 573–594. <https://doi.org/10.3390/molecules20010573>
- [17] P. Juárez *et al.*, "Halofuginone inhibits TGF- β /BMP signaling and in combination with zoledronic acid enhances inhibition of breast cancer bone metastasis," *Oncotarget*, vol. 8, no. 49, pp. 86447–86462, 2017. <https://doi.org/10.18632/oncotarget.21200>
- [18] S. Ahmad, H. W. Abbasi, S. Shahid, S. Gul, and S. W. Abbasi, "Molecular docking, simulation and MM-PBSA studies of Nigella sativa compounds: A computational quest to identify potential natural antiviral for COVID-19 treatment," *Journal of Biomolecular Structure and Dynamics*, vol. 39, no. 12, pp. 4225–4233, 2021.
- [19] V. d. S. Pinto *et al.*, "In silico study to identify new antituberculosis molecules from natural sources by hierarchical virtual screening and molecular dynamics simulations," *Pharmaceuticals*, vol. 12, no. 1, p. 36, 2019.
- [20] H. S. Roy, G. Dubey, V. K. Sharma, P. V. Bharatam, and D. Ghosh, "Molecular docking and molecular dynamics to identify collagenase inhibitors as lead compounds to address osteoarthritis," *Journal of Biomolecular Structure and Dynamics*, vol. 40, no. 5, pp. 2339–2351, 2022.
- [21] M. Doan, Huong Thi *et al.*, "Synthesis of febrifuginol analogues and evaluation of their biological activities," *Tetrahedron Letters*, vol. 55, no. 52, pp. 7226–7228, 2014.
- [22] A. Daina, O. Michielin, and V. Zoete, "SwissADME: A free web tool to evaluate pharmacokinetics, drug-likeness and medicinal chemistry friendliness of small molecules," *Scientific Reports*, vol. 7, no. 1, p. 42717, 2017.
- [23] J. H. Summerfield, "Simulation of 5-Fluorouracil Intercalated into Montmorillonite Using Spartan'14: Molecular Mechanics, PM3, and Hartree-Fock," *Open Journal of Physical Chemistry*, vol. 5, no. 03, p. 49, 2015.
- [24] B. F. Mohamed Thamby, V. M. Santhi, and A. Ramalingam, "Quantum chemical and experimental studies on the extraction of acid blue 80 and acid red 1 from their aquatic environment using tetrabutylammonium bromide based deep eutectic solvents," *Journal of Dispersion Science and Technology*, vol. 44, no. 9, pp. 1778–1787, 2023.
- [25] D. E. Pires, T. L. Blundell, and D. B. Ascher, "pkCSM: predicting small-molecule pharmacokinetic and toxicity properties using graph-based signatures," *Journal of Medicinal Chemistry*, vol. 58, no. 9, pp. 4066–4072, 2015.
- [26] N. Borkakoti *et al.*, "Structure of the catalytic domain of human fibroblast collagenase complexed with an inhibitor," *Nature Structural Biology*, vol. 1, no. 2, pp. 106–110, 1994.
- [27] G. Pochetti, R. Montanari, C. Gege, C. Chevrier, A. G. Taveras, and F. Mazza, "Extra binding region induced by non-zinc chelating inhibitors into the S1' subsite of matrix metalloproteinase 8 (MMP-8)," *Journal of Medicinal Chemistry*, vol. 52, no. 4, pp. 1040–1049, 2009.
- [28] S. J. Taylor *et al.*, "Fragment-based discovery of indole inhibitors of matrix metalloproteinase-13," *Journal of Medicinal Chemistry*, vol. 54, no. 23, pp. 8174–8187, 2011.
- [29] V. Schroder *et al.*, "Studies regarding the antimicrobial behavior of clotrimazole and limonene," *Antibiotics*, vol. 11, no. 12, p. 1816, 2022.
- [30] D. Van Der Spoel, E. Lindahl, B. Hess, G. Groenhof, A. E. Mark, and H. J. Berendsen, "GROMACS: Fast, flexible, and free," *Journal of Computational Chemistry*, vol. 26, no. 16, pp. 1701–1718, 2005.
- [31] M. J. Abraham *et al.*, "GROMACS: High performance molecular simulations through multi-level parallelism from laptops to supercomputers," *SoftwareX*, vol. 1, pp. 19–25, 2015.
- [32] P. Turner, *XMGRACE, version 5.1.19. Center for coastal and land-margin research, oregon graduate institute of science and technology*. USA: Beaverton, 2005.
- [33] R. Kumari, R. Kumar, O. S. D. D. Consortium, and A. Lynn, "G_mmpbsa □ A GROMACS tool for high-throughput MM-PBSA calculations," *Journal of Chemical Information and Modeling*, vol. 54, no. 7, pp. 1951–1962, 2014.
- [34] C. Wang, D. A. Greene, L. Xiao, R. Qi, and R. Luo, "Recent developments and applications of the MMPBSA method," *Frontiers in Molecular Biosciences*, vol. 4, p. 87, 2018.
- [35] T. K. Karami, S. Hailu, S. Feng, R. Graham, and H. J. Gukasyan, "Eyes on lipinski's rule of five: a new "rule of thumb" for physicochemical design space of ophthalmic drugs," *Journal of Ocular Pharmacology and Therapeutics*, vol. 38, no. 1, pp. 43–55, 2022.
- [36] Q. Zhang, J. Li, A. Middleton, S. Bhattacharya, and R. B. Conolly, "Bridging the data gap from in vitro toxicity testing to chemical safety assessment through computational modeling," *Frontiers in Public Health*, vol. 6, p. 261, 2018.
- [37] A. Tabernilla *et al.*, "In vitro liver toxicity testing of chemicals: A pragmatic approach," *International Journal of Molecular Sciences*, vol. 22, no. 9. <https://doi.org/10.3390/ijms22095038>
- [38] E. F. Ariyanto *et al.*, "Anthocyanin-containing purple sweet potato (*Ipomoea batatas* L.) synbiotic yogurt inhibited 3T3-L1 adipogenesis by suppressing white adipocyte-specific genes," *Journal of Experimental Pharmacology*, vol. 15, pp. 217–230, 2023. <https://doi.org/10.2147/JEP.S405433>